**SUPPLEMENTARY INFORMATION to**

# Controlling Charge Separation and Recombination by Chemical Design in Donor-Acceptor Dyads

Li Liu[1,*)], Pierre Eisenbrandt[2,*)], Thomas Roland[1)], Matthias Polkehn[2)], Pierre-Olivier Schwartz[1)], Kirsten Bruchlos[3)], Beatrice Omiecienski[3)], S. Ludwigs[3)], Nicolas Leclerc[4)], Elena Zaborova[4)*)], Jérémie Léonard[1)], Stéphane Méry[1)], Irene Burghardt[2,+)], Stefan Haacke[1,+)]

[1)] Institut de Physique et Chimie des Matériaux de Strasbourg & Labex NIE, Université de Strasbourg, CNRS UMR 7504, 23 rue du Loess, Strasbourg 67034, France
[2)] Institute for Physical and Theoretical Chemistry, Goethe University Frankfurt, Max-von-Laue-Str. 7, 60438 Frankfurt/Main, Germany
[3)] Institut für Polymerchemie, Universität Stuttgart, 70569 Stuttgart, Germany
[4)] ICPEES, Université de Strasbourg, CNRS UMR 7515, ECPM, 25 rue Becquerel, 67087 Strasbourg Cedex2, France

[+] Corresponding authors:
burghardt@chemie.uni-frankfurt.de
stefan.haacke@ipcms.unistra.fr

*These authors contributed equally to this work

[*] New address: CiNaM, Aix Marseille Université, CNRS UMR 7325, Campus de Luminy, 13288 Marseille, France

## Contents



## 1) Global Analysis of the transient absorption data: Example $D_1\delta A$

After the processing of chirp and solvent correction as described in refs. 1,2, the transient absorption data is subjected to singular value decomposition (SVD) to reduce the noise level by rejection of higher order eigencomponents. The five first components (kinetic traces multiplied by eigenvalues) are taken and fitted with the same time constants but different amplitudes according to $\Delta A(\lambda,t) = \sum_i A_i(\lambda) e^{-t/\tau_i}$.

**Figure S1** shows these traces and their fits for $D_1\delta A$ in chloroform (DA spectra in **fig. 3**).

A minimum of five time constants is necessary and the fitting parameters are in **Table S1**. The Decay-associated difference spectra (DADS) are reconstituted based on the fitting as shown in **Fig S2**.

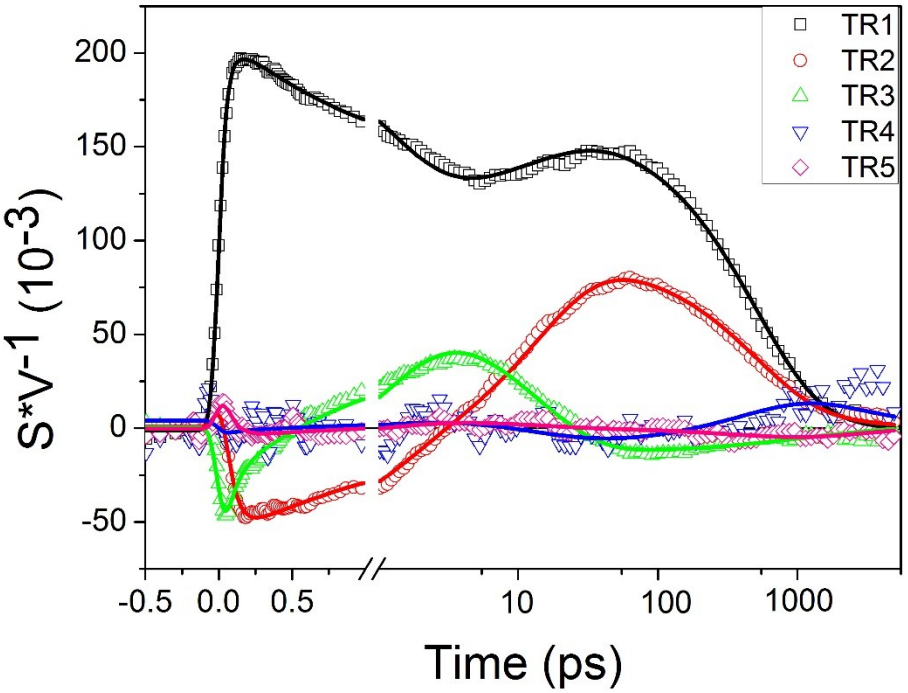


**Fig S1.** Global Analysis of $D_1\delta A$ in chloroform for the first five components after S.V.D. The open symbols are kinetic traces multiplied by S value (black square for the first component, red circle for second, green up-triangle for third, blue down-triangle for the fourth and pink diamond for the fifth) with their fits (corresponding colors).

**Table S1.** Fitting parameters for the five principal kinetic traces obtained by SVD analysis for DδA in chloroform.

| | TR1 | TR2 | TR3 | TR4 | TR5 |
|---|---|---|---|---|---|
| DAS1-60fs | -0.050 | 0.115 | -0.055 | -0.003 | 0.011 |
| DAS2-1.2ps | 0.090 | -0.043 | -0.091 | -0.009 | 0.002 |
| DAS3-14ps | -0.040 | -0.106 | 0.074 | 0.004 | 0.002 |
| DAS4-500ps | 0.149 | 0.078 | -0.005 | 0.009 | 0.005 |
| DAS5-2.2ns | 0.013 | 0.011 | -0.008 | -0.009 | 0.005 |

As described in the main text, these DADS also support the reaction scheme deduced from the raw data. Since the lifetime of DADS1, 60 fs, is too close to IRF, the spectral features are a mixture of artifacts, due to pump and probe cross-phase modulation, relaxation of the GSB spectrum of D, and rise of the ESA of D* (>700nm). Consequently, the 60-fs spectral evolution is due to D* excited state equilibration. DADS2 (1.2 ps) shows the energy transfer from donor to acceptor, as the GSB of the donor decays in the 400 to 500 nm range and the GSB, SE and ESA of the acceptor are formed (peaks at 490, 535, 575 and 705 nm). In DADS3, the positive band from 400 to 500 nm means reformation of donor GSB to form the CT state (peaks at 719 and 806 nm). The negative peaks at 535 and 575 nm due to the decay of the SE also

confirm this process. DADS4 matches with spectro-electro-chemistry measurement as shown in **fig 4** and represent the CT state decay. The long-lived DADS5 has the same spectral form as DADS4 with a 10 times less amplitude, and is probably due to a minority longer-lived molecular conformation of the same CT state.

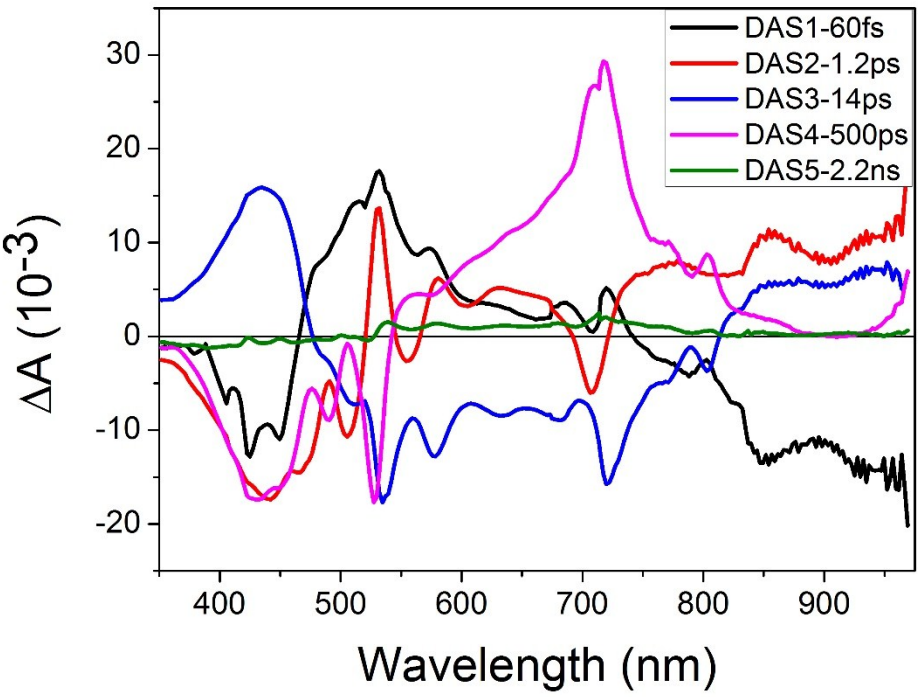


**Figure S2**. Decay-associated differential spectrum (DADS) of DδA obtained by global analysis.

**Figure S3** shows the good quality of the global fit for kinetic traces at three selected wavelengths, that represent the ground state bleach recovery of $D_1$ and A, and the transition from the excited state to the anionic absorption signatures.

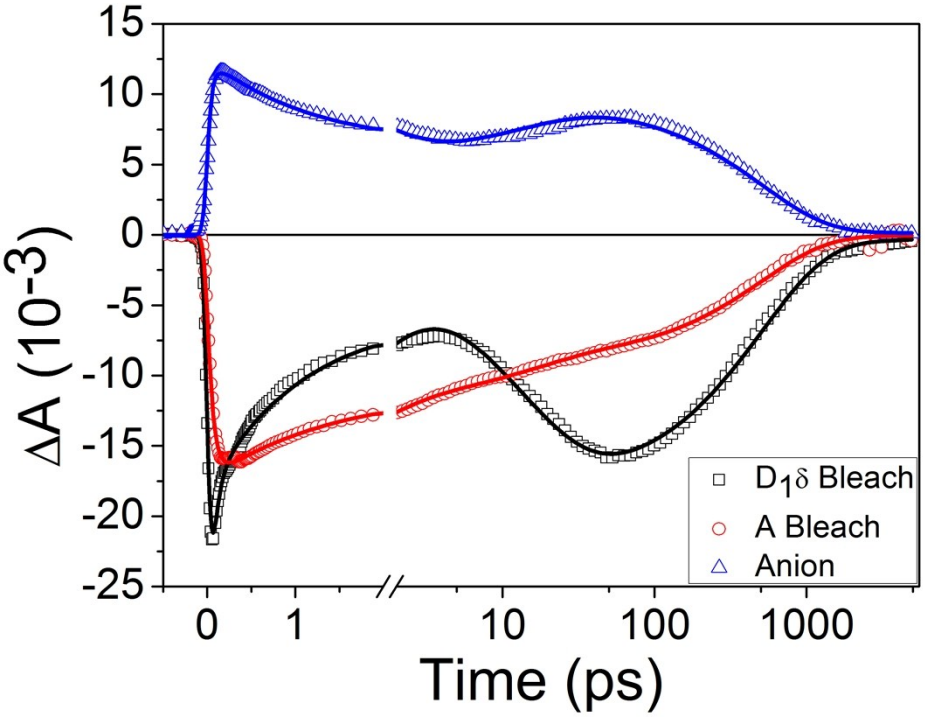


**Figure S3.** Selected kinetic traces (symbols) and global fit (lines) observed for A$\delta$D$_1$ in chloroform and corresponding to the donor GSB at 430 nm (black), the acceptor GSB at 490 nm (red) and the anion signature at 800 nm (blue).

## 2) Effect of the donor length in the $D_n\delta_+A$ molecules

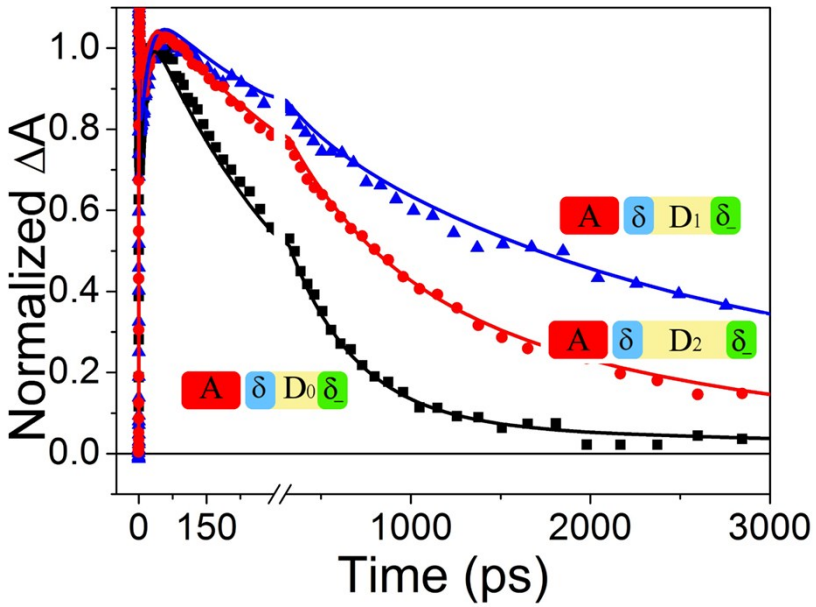


**Figure S4:** Kinetic traces at 800nm: Effect of donor length for the $D_n\delta_+A$ molecules, with n = 0 (black), 1 (red), 2 (blue) or 3 (pink). The donor length almost has no effect on the CT formation and recombination times for molecules without $\delta_-$ when n >1. The CT dominant lifetime decreases by about 10% when n=0.

## 3) Marcus-Jortner analysis

**Table S2**. Parameters and molecular reorganization energies used in the Marcus-Jortner model. r+ , r- and $R_{CC}$ are taken as the hole, electron density radii and the distance between electron and hole density centers as calculated from electronic structure modeling (see paper). $E_{red}$ and $E_{ox}$ are the oxidation and reduction potential energies determined experimentally (see paper). $E_{00}$ is the lowest excited state, from which the CT states are formed. $\lambda_{mol}$ is the computed molecular reorganization energy for charge recombination and charge formation.

| | $D_1\delta A$ | $D_1\delta_+ A$ | $\delta_- D_1\delta_+ A$ |
|---|---|---|---|
| $r_+$ (nm) | 0.8 | 0.7 | 0.9 |
| $r_-$ (nm) | 0.4 | 0.4 | 0.4 |
| $R_{cc}$ (nm) | 2.3 | 2.2 | 2.5 |
| $E_{red}$ (eV) | -0.40 | -0.40 | -0.40 |
| $E_{ox}$ (eV) | 0.89 | 0.89 | 0.81 |
| $E_{00}$ (eV) | 2.32 | 1.92 | 1.92 |
| $\lambda_{mol}$ (eV) Formation | *0.33* | 0.30 | 0.28 |
| $\lambda_{mol}$ (eV) Recombination | 0.57 | 0.68 | 0.69 |

**Table S3.** Estimated solvent reorganization energies $\lambda_{sol}$ (Eq. 3, see paper) and Gibbs free energies for charge recombination $\Delta G^0_{CR}$ (Eq. 4) and for charge separation $\Delta G^0_{CS}$ (Eq.5)

| | | Toluene | TCE | Chloroform |
|---|---|---|---|---|
| ε | | 3.5 | 3.42 | 4.89 |
| n | | 1.496 | 1.477 | 1.446 |
| $D_1\delta A$ | $\lambda_{sol}$ (eV) | 0.333 | 0.344 | 0.568 |
| | $-\Delta G^0_{CS}$ (eV) | 0.739 | 0.725 | 0.907 |
| | $\lambda_{CS}=\lambda_{mol}+\lambda_{sol}$ (eV) | 0.663 | 0.674 | 0.898 |
| | $-\Delta G^0_{CR}$ (eV) | 1.580 | 1.594 | 1.412 |
| | $\lambda_{CR}=\lambda_{mol}+\lambda_{sol}$ (eV) | 0.903 | 0.914 | 1.138 |
| $D_1\delta_+ A$ | $\lambda_{sol}$ (eV) | 0.349 | 0.360 | 0.595 |
| | $-\Delta G^0_{CS}$ (eV) | 0.323 | 0.309 | 0.500 |
| | $\lambda_{CS}=\lambda_{mol}+\lambda_{sol}$ (eV) | 0.649 | 0.660 | 0.895 |
| | $-\Delta G^0_{CR}$ (eV) | 1.594 | 1.609 | 1.418 |
| | $\lambda_{CR}=\lambda_{mol}+\lambda_{sol}$ (eV) | 1.029 | 1.040 | 1.275 |
| $\delta_- D_1\delta_+ A$ | $\lambda_{sol}$ (eV) | | | 0.554 |
| | $-\Delta G^0_{CS}$ (eV) | | | 0.585 |
| | $\lambda_{CS}=\lambda_{mol}+\lambda_{sol}$ (eV) | | | 0.834 |
| | $-\Delta G^0_{CR}$ (eV) | | | 1.333 |
| | $\lambda_{CR}=\lambda_{mol}+\lambda_{sol}$ (eV) | | | 1.244 |

## 4) Details of electronic structure analysis

### 4.1) Benchmark and comparison of several DFT functionals

Since all of the above donor-acceptor combinations represent very large molecular species, the application of high-level ab-initio methods was only possible to a limited extent. As a consequence, only a relatively small basis set could be employed. Here, we present benchmark results for the $D_0\delta_+A$ species; similar results were obtained for the $D_0\delta A$ and $\delta_-$ species. The CC2/SVP and ADC2/SVP methods both show similar transitions. Unfortunately for CC2/SVP no oscillator strengths could be obtained. The order of the interesting states according to CC2/SVP is given as $DS_1<AS_1<CT<DS_2$. ADC2/SVP however changes the $DS_1$ and $AS_1$ excitations, and the $AS_1$ excitation shows a large oscillator strength while the one for $DS_1$ is rather small. Furthermore both excitations show a pronounced mixing (about 65/35), since they are excitonically coupled and form a J-type aggregate. From this, one can infer that in our CC2/SVP calculations, the lowest (nominally $DS_1$) excitation should exhibit a large oscillator strength while the second (nominally $AS_1$) excitation should have a relatively small oscillator strength. The corresponding orbitals are shown in **Figure 3** of the manuscript.

**Table S4.** Results for $D_0\delta_+A$ with CC2/SVP. (The oscillator strength could not be obtained.)

| State | Excitation energy [eV] | $f_{osc}$ | MO expansion coefficients | Location |
|---|---|---|---|---|
| **1** | 2.75 ($DS_1$) | --- | H>L+1 (0.861)<br>H-2>L (-0.404) | D>$\delta_+$<br>(A>A) |
| **2** | 2.81 ($AS_1$) | --- | H-2>L (0.893)<br>H>L+1 (0.398) | A>A<br>(D> $\delta_+$) |
| **3** | 2.99 ($CT_1$) | --- | H>L (0.950)<br>H-1>L (0.281) | D>A |
| **4** | 3.55 | --- | H-1>L+1 (-0.861)<br>H-3>L+1 (0.400) | D> $\delta_+$ |
| **5** | 3.65 | --- | H-1>L (-0.632)<br>H-13>L (0.516) | D>A<br>(A>A) |
| **6** | 3.67 | --- | H-13>L (0.656)<br>H-1>L (0.514) | A>A<br>(D>A) |
| **7** | 3.70 | --- | H-24>L (0.846) | D>A |
| **8** | 3.71 | --- | H-22>L (0.845) | A>A |
| **9** | 3.77 ($DS_2$) | --- | H>L+4 (0.896) | D>D |
| **10** | 3.90 | --- | H-14>L (-0.791) | A>A |

**Table S5.** Results for $D_0\delta_+A$ with ADC2/SVP.

| State | Excitation energy [eV] | $f_{osc}$ | MO expansion coefficients | Location |
|---|---|---|---|---|
| **1** | 2.73 ($AS_1$) | 2.29 | H-2>L (0.0.779)<br>H>L+1 (-0.576) | A>A<br>(D> $\delta_+$) |
| **2** | 2.77 ($DS_1$) | 0.28 | H>L+1 (0.747)<br>H-2>L (0.604) | D>$\delta_+$<br>(A>A) |
| **3** | 2.96 ($CT_1$) | 0.0 | H>L (0.949)<br>H-1>L (0.284) | D>A |
| **4** | 3.50 | 0.0 | H-23>L(0.854) | A>A |
| **5** | 3.51 | 0.0 | H-22>L (0.853) | A>A |
| **6** | 3.55 | 0.01 | H-1>L +1(-0.824) | D> $\delta_+$ |
| **7** | 3.59 | 0.0 | H-1>L (-0.810) | D>A |
| **8** | 3.66 | 0.0 | H-13>L (0.795)<br>H-2>L+5 (0.479) | A>A |
| **9** | 3.80 ($DS_2$) | 1.19 | H>L+4 (0.882) | D>D |
| **10** | 3.87 | 0.01 | H-14>L (-0.719) | A>A |

These results were then used as a benchmark to assess several DFT functionals as well as the CIS method. **Figure S5** gives an overview of these results. Only the relevant states were plotted. In general we found that that DFT and CIS locate the $DS_1$ excitation below the $AS_1$ excitation. Furthermore, since these two are less energetically close there is only a small (e.g. wB97XD) or even no coupling (e.g. CAM-B3LYP). The description of charge transfer states with linear response TD-DFT is problematic, because of the electron-transfer self-interaction (ET-SI) error of linear response TD-DFT. This deficiency can be corrected with a higher fraction of Hartree-Fock (HF) exchange (BHLYP,B575LYP) and long-range corrected functionals (wB97XD, CAM-B3LYP). One can see that the excitation energy of the CT state rises with increasing HF exchange. While wB97XD gives a small mixing between $AS_1$ and $DS_1$, the CT state is described above the $DS_2$ state, whereas the ordering is correct for B575LYP and CAM-B3LYP. The B575LYP functional was employed since this functional was used successfully in the description of a precursor donor acceptor dyad[3]. CIS does give good results for the ordering of the $AS_1$, $DS_1$ and $DS_2$ states, but does not show any mixing of $AS_1$ and $DS_1$, and the CT state is given at a too high energy. From these results we concluded that a reasonable procedure is to (i) carry out geometry optimizations with the wB97XD functional and (ii) subsequently use the CAM-B3LYP functional for the description of the excited states, based on the wB97XD structure.

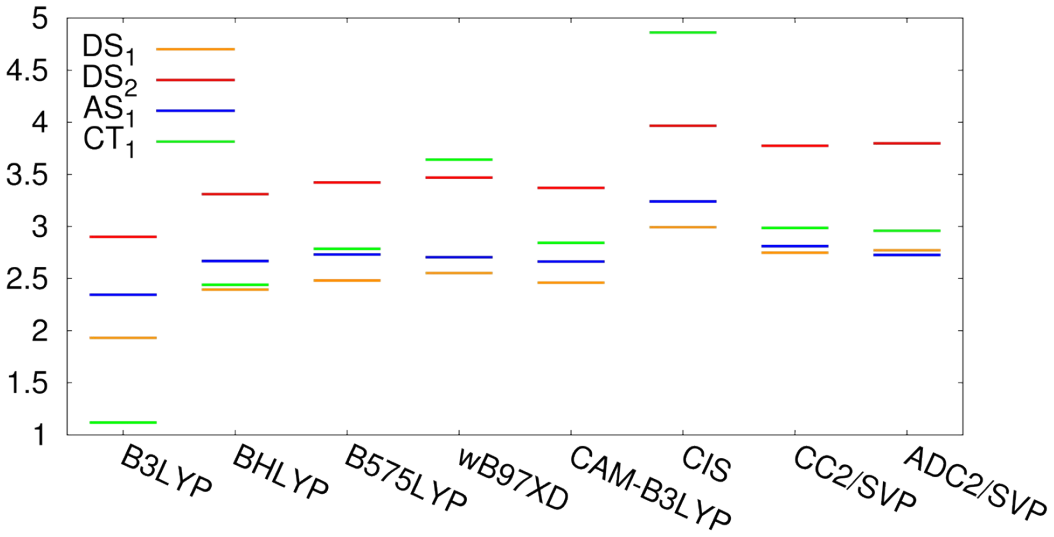


**Figure S5.** Comparison of different methods and DFT functionals for $D_0\delta_+A$ in vacuum. The CC2/SVP method has been used as a benchmark.

**Table S6.** Results for $D_0\delta_+A$ with wB97XD/TZVP.

| State | $E_x$ [eV] | $f_{osc}$ | MO share [%] | Location |
|---|---|---|---|---|
| **1** | 2.55 ($DS_1$) | 1.84 | H>L+1 (84.9) | D> $\delta_+$ |
| **2** | 2.70 ($AS_1$) | 0.58 | H-2>L (97.0) | A>A |
| | | | H+1 (3.0) | |
| **3** | 3.47 ($DS_2$) | 0.58 | H>L+4 (52.5) | D>D |
| | | | H-1>L+1 (34.7) | |
| **4** | 3.50 ($CT_1$) | 0.00 | H>L(90.2) | D>A |
| **5** | 3.78 | 0.00 | H-13>L (64.8) | A>A |
| **6** | 3.84 | 0.70 | H-1>L +1(30.8) | D>D |
| | | | H>L+4 (0.24.9) | |
| **7** | 3.96 | 0.00 | H-2>L+3 (35.6) | A>A |
| | | | H-2>L+5 (30.9) | |
| **8** | 4.00 | 0.01 | H-14>L (69.1) | A>A |
| **9** | 4.09 | 0.00 | H-17>L (36.5) | A>A |
| | | | H-16>L (35.6) | |
| **10** | 4.12 | 0.00 | H-19>L (68.8) | A>A |

**Table S7.** Results for $D_0\delta^+A$ with CAM-B3LYP/TZVP.

| State | $E_x$ [eV] | $f_{osc}$ | MO share [%] | Location |
|---|---|---|---|---|
| **1** | 2.46 ($DS_1$) | 1.69 | H>L+1 (92.8) | D> $\delta_+$ |
| **2** | 2.66 ($AS_1$) | 0.66 | H-2>L (100.0) | A>A |
| **3** | 2.84 ($CT_1$) | 0.00 | H>L (96.3) | D>A |
| **4** | 3.37 ($DS_2$) | 0.42 | H-1>L+1(49.7) | D>D |
| | | | H>L+4 (40.1) | |
| **5** | 3.51 | 0.00 | H-1>L (90.2) | D>A |
| **6** | 3.62 | 0.77 | H>L +4(44.5) | D>D |
| | | | H-1>L+1 (31.0) | |
| **7** | 3.74 | 0.00 | H-13>L (68.1) | A>A |
| **8** | 3.91 | 0.00 | H-2>L+3 (36.3) | A>A |
| | | | H-15>L (27.7) | |
| **9** | 3.98 | 0.05 | H-14>L (71.9) | A>A |
| **10** | 4.12 | 0.00 | H>L+6 (67.2) | D>D |

### 4.2) Electron/hole densities

The electron/hole densities presented here are comparable to attachment/detachment densities, but are calculated differently. For further details see the Multiwfn documentation.[4,5] In the following, the hole>electron density plots are shown for the relevant states described above. By comparing $D_0\delta_+A$ (**Figure S6**) and $\delta_-D_0\delta_+A$ (**Figure S7**) one can see that the densities for excitations $AS_1$ and $DS_1$ are almost identical. By contrast, $DS_2$ and $CT_1$ show changes in the hole-densities. **Figure S7** shows that the addition of the $\delta_-$ group does influence the $DS_2$ and $CT_1$ hole-densities, such that the densities are extended towards the $\delta_-$ group, which reflects the increase of $R_{CC}$. The electron-densities are again almost identical.

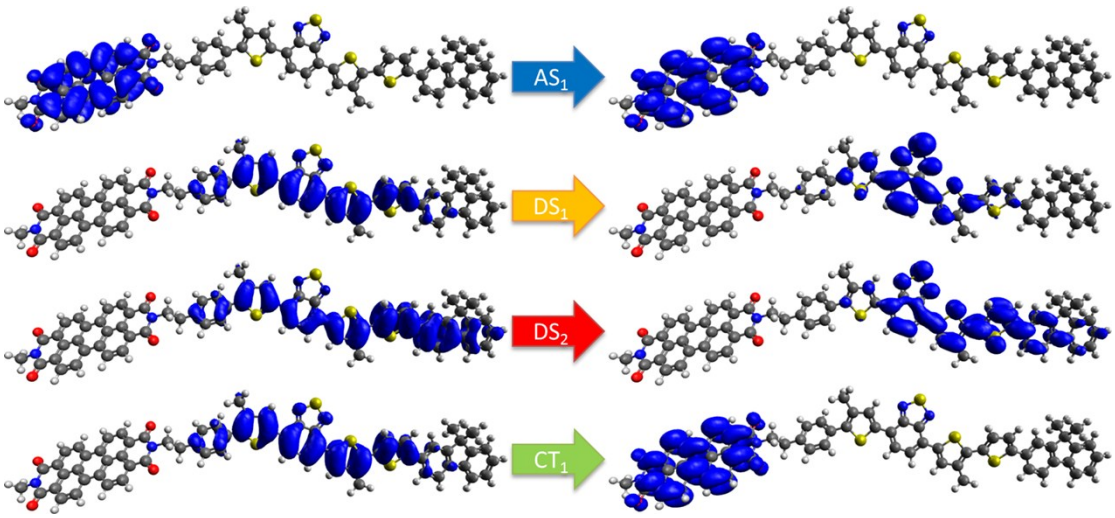


**Figure S6.** Electron density changes associated with the optical transitions for $D_0\delta_+A$

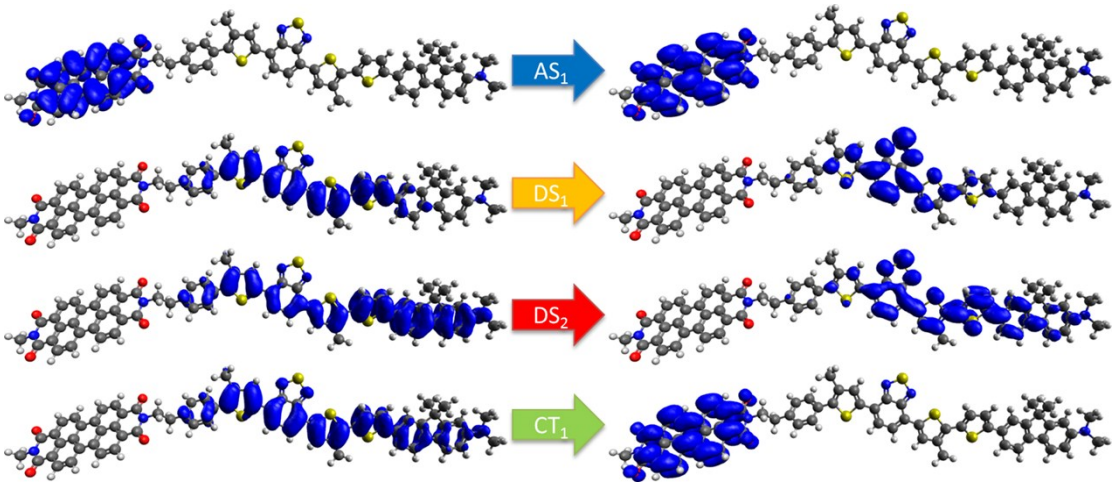


**Figure S7.** Electron density changes associated with the optical transitions for $\delta^{-}D_0\delta_{+}A$

### 4.3) Excited state geometry optimizations

In order to explore a possible photochemical pathway, excited state geometry optimizations have been carried out. From these, the approximate values for $\lambda_{mol}$ are extracted. **Figures S8** and **S9** refer to $D_0\delta_{+}A$. **Figure S8** shows the excitation energies for the different optimized structures and **Figure S9** depicts the relative energies of the different states. As reference the ground state (GS) energy of the GS structure has been used and all energies are plotted relative to this energy. **Figures S10** and **S11** show the same information for $\delta_{-}D_0\delta_{+}A$.

**Figure S9** and **S11** both show similar results. The ordering of the states (except for $CT_2$) is identical. Starting with the $DS_2$ excitation in the GS structure one could infer that either a very fast transfer to $DS_1$ sets in (in accordance with the experimental results) or the molecule first relaxes to the $DS_2$ structure, followed by a transfer to $DS_1$. Regarding the composition of the state transitions, we can see a mixing of $DS_1$ and $DS_2$ already in the GS structure (75:25). In the $DS_2$ structure, the mixing nearly remains the same (80:20). Here we might have a possible "transfer channel" from the $DS_2$ to the $DS_1$ state. The experiments performed on $D_0\delta_{+}$ or $D_1\delta_{+}$indicate indeed that this energetic relaxation occurs within 0.2 ps (unpublished results), leading then to emission from $\delta_{+}$ ($DS_1$) as can be seen for $D_1\delta_{+}A$. in **Figure 8** (trough at 600-700 nm). From the theory side, a clear-cut answer cannot be given between these two pathways - i.e., fast transfer to $DS_1$ or initial relaxation. A crossing between the $DA_1$ and $DS_2$ is likely, but was not observed.

From the $DS_1$ state, neither a transition to the CT state nor transitions to any other excited state are possible, at least as far as we can conclude from our vacuum calculations. As already shown in the main text (**Figure 4**), the situation can change when including solvation effects (via COSMO, implemented in ORCA[6]): Now, the CT state moves below the $DS_1$ state and an energy transfer is possible (compare Ref. [3]).

One should note that these optimized structures only represent special points on the potential energy surface (PES). For the calculated points, each state reaches an energetic minimum in its optimized excited state geometry. However, because of the

huge number of degrees of freedom (DOF) in the molecule these structures very likely represent only local minima. Due to the limited information on the high-dimensional PES, we cannot exclude, e.g., the presence of a crossing between $DS_1$ and $DS_2$, even though we have no direct evidence of such a crossing (we only see a mixing in the MO expansion coefficients).

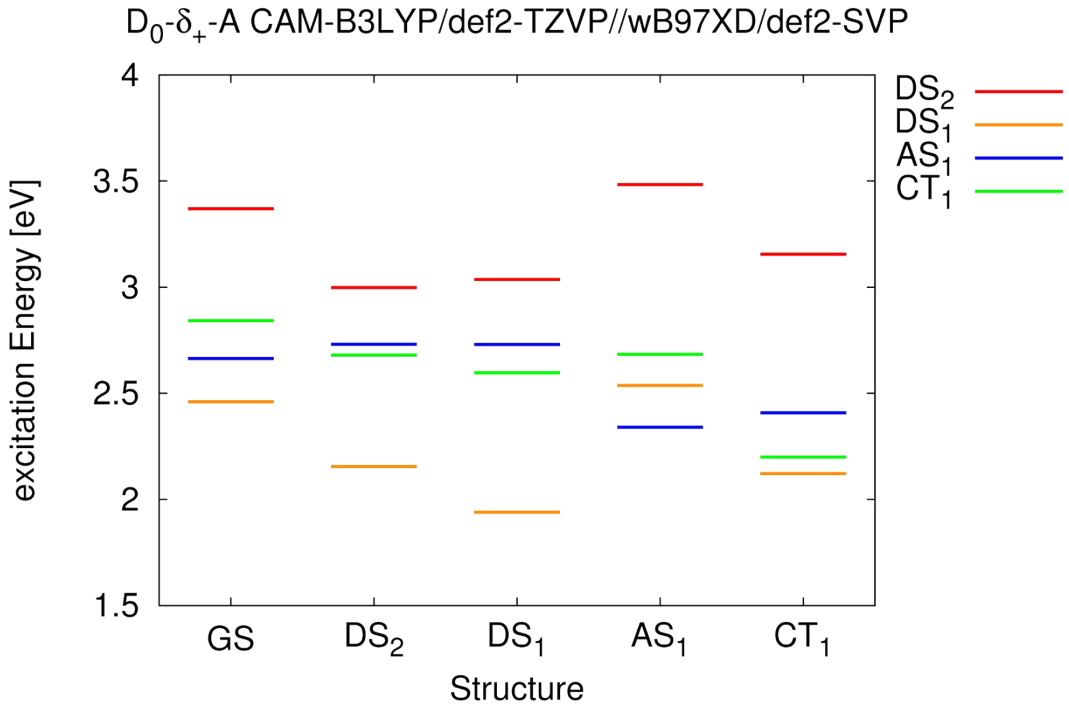


**Figure S8.** Excitation energies of the relevant states within the optimized structures (bottom) of these states in vacuum.

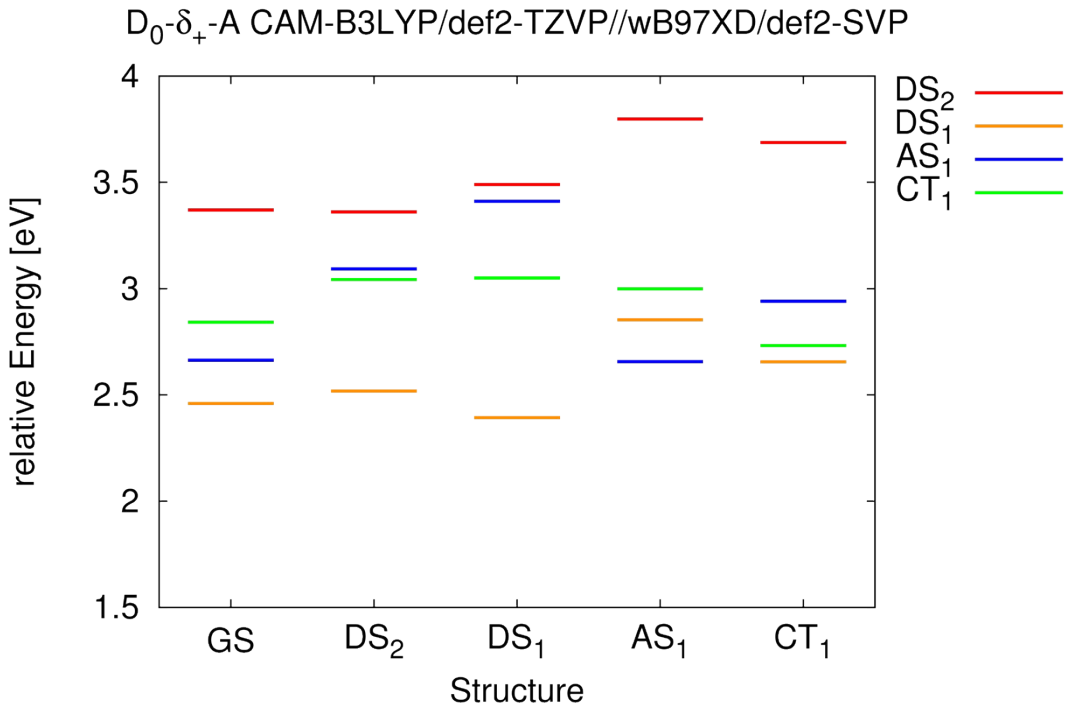


**Figure S9.** Relative energy of the relevant states for the optimized structures of these states in vacuum.

All energies are plotted relatively to the ground state energy of the ground state structure.

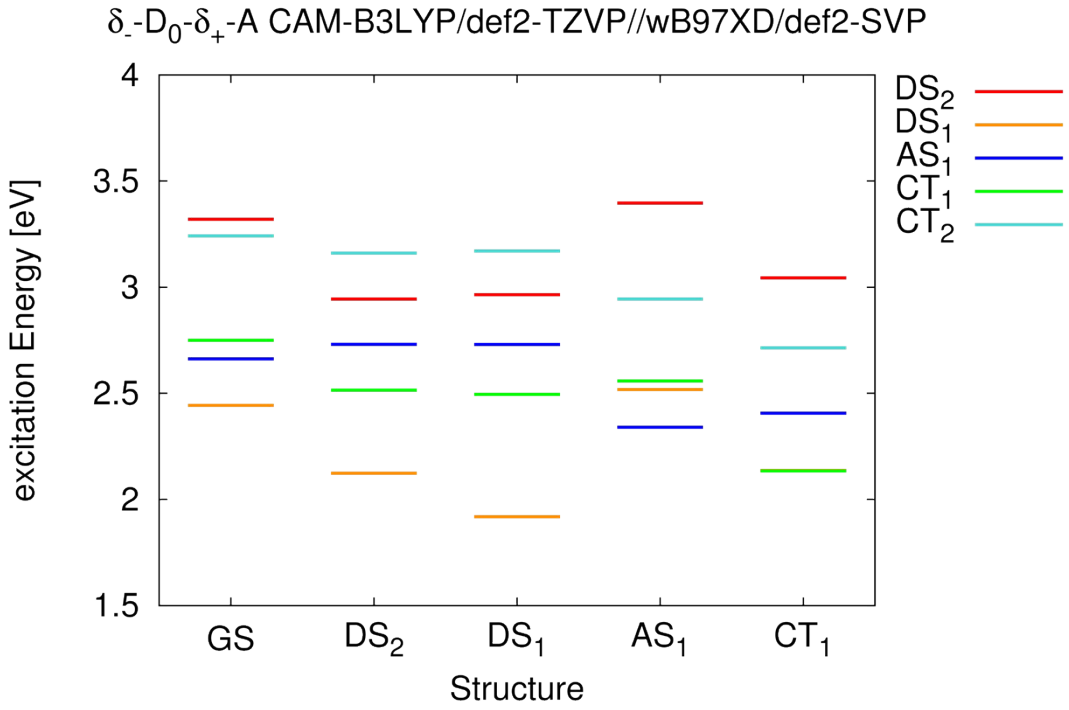


**Figure S10.** Excitation energies of the relevant states on the optimized structures of these states in vacuum.

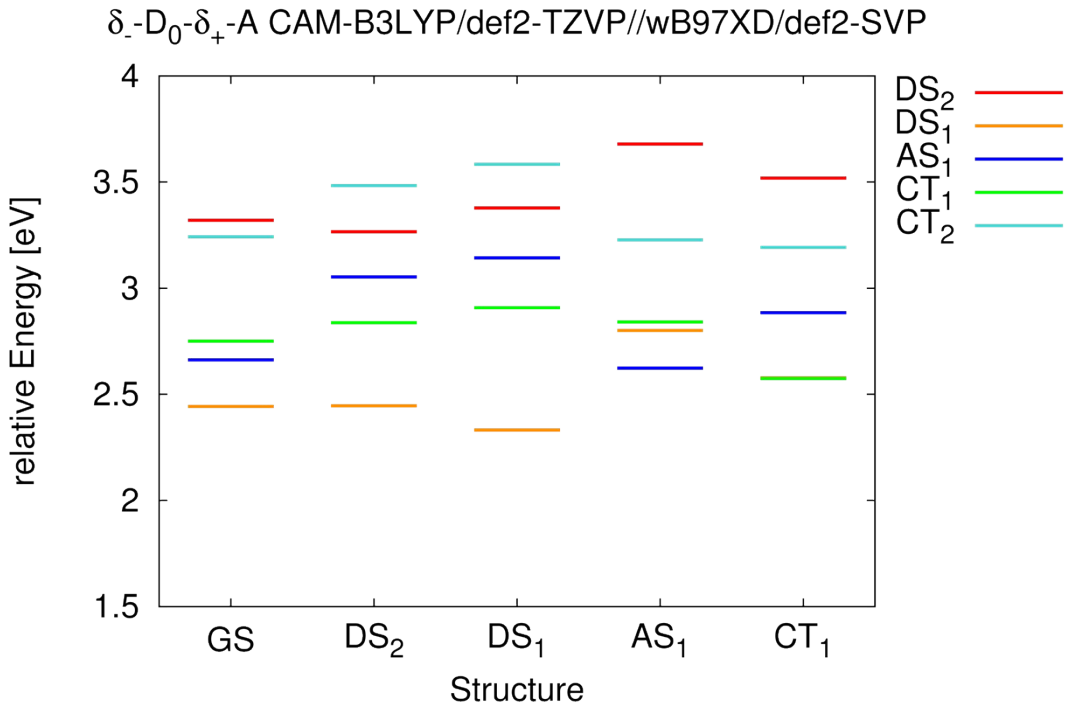


**Figure S11.** Relative energy of the relevant states for the optimized structures of these states in vacuum. All energies are plotted relatively to the ground state energy of the ground state structure.

### 4.4) Dipole moments

Dipole moments were calculated for the isolated donor and acceptor species. The

donor species were considered in their cationic form (i.e., carrying a hole) while the acceptor species were considered in their anionic form (i.e., carrying an extra electron), suitable to describe a charge transfer state. The results are shown in **Table S8**. Furthermore, we calculated the dipole moment for the complete dyad in the charge transfer state. For these cases, one evidently finds a high dipole moment arising from the charge separation. Looking at the results, we see that increasing the donor length (n=0 >n=1) leads to an increase of the dipole moment. Changing the δ part to $\delta_+$ decreases the dipole moment for the short donors (n=0) and increases the dipole moment for the long (n=1) donors. Addition of the $\delta_-$-group leads to an increase of the dipole moment (larger increase for n=0).

However, these results do not yet inform about the direction of the dipole moment. One sees for the donors without $\delta_-$, that the dipole moment does not point in the same direction (the angles between the vectors range from 45° to 180°). For the donors with the $\delta_-$-group the vectors approximately show in the same direction (~0°-10°). One can think of this as a CT state located on the donor, where the "electron" is on the $\delta_+$-group and the "hole" on the $\delta_-$-group. Therefore in the CT-State of the dyad the electron located on the acceptor and the hole located on the donor are more separated (which fits with the mixing of the $CT_1$ and $CT_2$ states).

**Table S8.** Comparison of the dipole moments for the charged acceptor and donor moieties and the dyads in the CT-state.

| Molecule | „State" | Dipole [Debye] | approx. angle between DM |
|---|---|---|---|
| **Acceptor** | anionic | 0,11 | --- |
| **D0-δ** | cationic | 3.05 | 45° |
| **D1-δ** | cationic | 14.34 | 180° |
| **D0-$\delta_+$** | cationic | 1,77 | 90° |
| **D1-$\delta_+$** | cationic | 28,56 | 135° |
| **$\delta_-$-D0-δ** | cationic | 21.55 | 0°-10° |
| **$\delta_-$-D1-δ** | cationic | 45.60 | 10°-20° |
| **$\delta_-$-D0-$\delta_+$** | cationic | 12,82 | 0°-10° |
| **$\delta_-$-D1-$\delta_+$** | cationic | 30,88 | 0°-10° |
| | | | |
| **D0-δ-A** | CT | 99.22 | --- |
| **D1-δ-A** | CT | 108.55 | --- |
| **D0-$\delta_+$-A** | CT | 85.02 | --- |
| **D1-$\delta_+$-A** | CT | 85.57 | --- |
| **$\delta_-$-D0-δ-A** | CT | 108.90 | --- |
| **$\delta_-$-D1-δ-A** | CT | 86.08 | --- |
| **$\delta_-$-D0-$\delta_+$-A** | CT | 100.53 | --- |
| **$\delta_-$-D1-$\delta_+$-A** | CT | 84.46 | --- |

### 4.5) Reaction pathway for $\delta_{-}D_0\delta_{+}A$ species

Analogously to Figure 9 of the main text, the results of geometry optimizations are shown in Figure S12 for the $\delta_{-}D_0\delta_{+}A$ species. As can be seen by comparing the figures, the excited-state pathways are not significantly altered by adding the $\delta_{-}$ moiety.

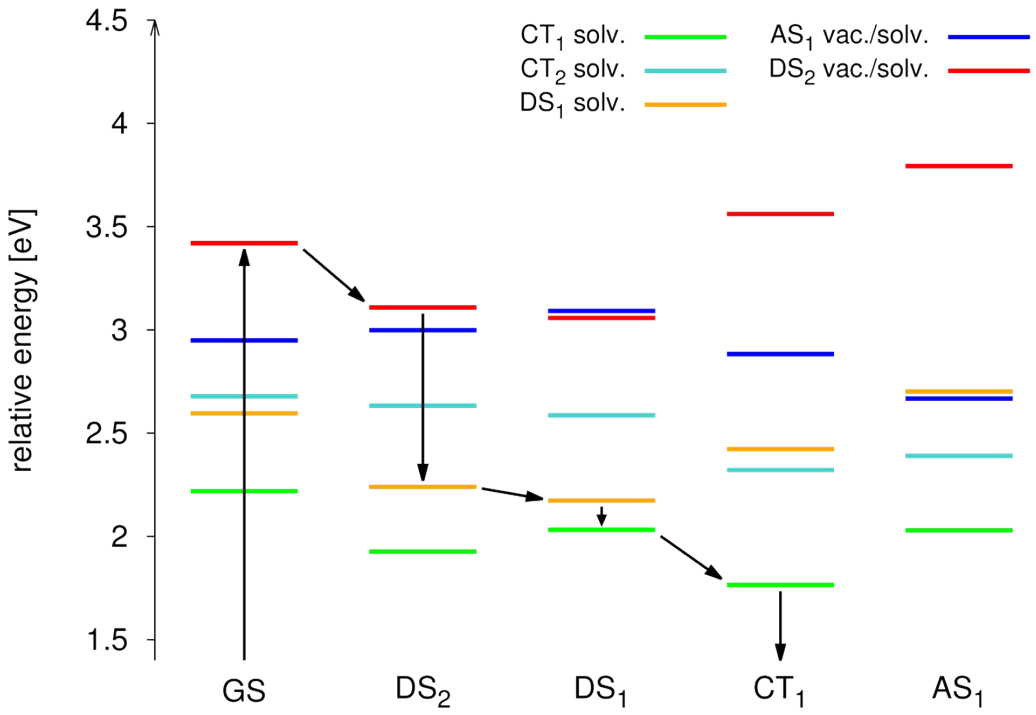


**Figure S12.** Illustration of possible photochemical pathway for the $\delta_{-}D_0\delta_{+}A$ species, obtained by state-specific geometry optimization, analogously to the results reported in **Figure 9** of the main text for the $D_0\delta_{+}A$ species.

## References


1. J. Briand, O. Bram, J. Rehault, J. Leonard, A. Cannizzo, M. Chergui, V. Zanirato, M. Olivucci, J. Helbing and S. Haacke, *Phys. Chem. Chem. Phys.*, 2010, **12**, 3178-3187.
2. T. Roland, PhD thesis, University of Strasbourg, 2014 https://tel.archives-ouvertes.fr/tel-01079791.
3. J. Wenzel, A. Dreuw and I. Burghardt, *Phys. Chem. Chem. Phys.*, 2013, **15**, 11704.
4. L. Lu, T. Zheng, Q. Wu, A. M. Schneider, D. Zhao and L. Yu, *Chem. Rev.*, 2015, **115**, 12666-12731.
5. T. Lu and F. Chen, *J. Comput. Chem.*, 2012, **33**, 580-592.
6. F. Neese, *WIREs Comput Mol Sci*, 2012, **2**, 73-78.